OPAL Physics Note PN-282
6 March 1997

Search for Unstable Neutral and Charged Heavy Leptons in e^+e^- collisions at $\sqrt{s} = 170$ and 172 GeV

The OPAL Collaboration

Abstract

Searches for an unstable neutral heavy lepton (N) and for a charged heavy lepton ($L^\pm$) have been performed using a data sample of 10.4 pb^{-1} at a centre-of-mass energy of $\sqrt{s} = 170$ and 172 GeV collected with the OPAL detector at LEP in 1996. We study the signal $e^+e^- \to N\bar{N}$ where the neutral heavy lepton decays into only one of the standard light charged lepton species and an off-shell W boson. For a Dirac type N a lower limit on m_N at 95 % C.L. is 79.1 GeV if $N \to e\,W^*$, 78.5 GeV if $N \to \mu\,W^*$ and 69.0 GeV if $N \to \tau\,W^*$; for a Majorana type N the limits obtained are 69.8 GeV and 68.5 GeV respectively for the cases $N \to e\,W^*$ and $N \to \mu\,W^*$ (for the case $N \to \tau\,W^*$ the limit is not improved compares to the previous analysis done at 161 GeV). For a charged heavy lepton we study the process $e^+e^- \to L^+L^-$. A lower limit obtained at 95 % C.L. for m_L is 81.4 GeV if $L^- \to N\,W^{-*}$ (with $m_N < 63.9$ GeV, and N stable within the detector volume), and 80.2 GeV if $L^- \to \nu_\ell W^{-*}$.

This note describes preliminary OPAL results to be submitted to the XVIII International Symposium on Lepton-Photon Interactions, Hamburg, 28 July - 1 August 1997

1 Introduction

It is well known that, in spite of its remarkable success in describing all experimental electroweak data available today, the Standard Model (SM) leaves many questions unanswered. In particular, it does not explain the number of fermion generations nor the mass spectrum. Here, we are interested in the possible existence of heavy fermions, as predicted by extensions of the Standard Model. These new fermions could be of the following types (for a review see [1]): (i) sequential fermions (the existence of a fourth generation is still allowed if the associated neutral lepton is heavy enough), (ii) mirror fermions (with chirality opposite to those of the SM), (iii) vector fermions (with left and right-handed doublets), and (iv) singlet fermions. These new fermions could be produced at high energy e^+e^- colliders such as LEP, via the $\gamma^* Z^0$ exchange assuming standard coupling, where two production mechanisms are possible: (i) pair production, and (ii) single production in association with a light standard fermion from the three known generations.

At LEP 1, such fermions have been excluded up to a mass of ~ 46.5 GeV [2]. The high energy upgrade of LEP (LEP 2) which achieved $\sqrt{s} = 161$ GeV during the summer of 1996 [3] has pushed the limit on the masses to around ~ 70 GeV for a neutral heavy lepton and about ~ 75 GeV for a charged one.

We present here a model independent search for neutral and charged heavy lepton pair production ($\mathrm{N\bar{N}}$ and $\mathrm{L^+L^-}$) in e^+e^- collisions. The data were recorded by the OPAL experiment at LEP during October and November of 1996, for an integrated luminosity of 10.4 pb^{-1} at $\sqrt{s} = 170.3$ and 172.3 GeV. We consider here unstable heavy leptons (a stable neutral heavy lepton is disfavoured on cosmological and astrophysical grounds [4]). To avoid leptonic flavor changing neutral currents (FCNC) at the one-loop level, we assume a coupling with only one of the light standard leptonic generations via mixing. Heavy leptons can decay through the charge current (CC) or the neutral current (NC) channels:

$$\mathrm{N} \to \ell^\pm \mathrm{W}^{\mp *} \quad , \quad \mathrm{N} \to \nu_\ell \mathrm{Z}^*$$
$$\mathrm{L}^\pm \to \nu_\ell \mathrm{W}^{\pm *} \quad , \quad \mathrm{L}^\pm \to \mathrm{N W}^{\pm *} \quad , \quad \mathrm{L}^\pm \to \ell^\pm \mathrm{Z}^*$$

where $\ell = \mathrm{e}$, μ or τ; and branching ratios are respectively $\sim \frac{3}{4}$ for CC and $\sim \frac{1}{4}$ for NC and for a heavy lepton mass $\gg M_\mathrm{W}$. Expressions for the computation of partial decay widths with off-shell W's and Z's can be found in [5]. A mixing angle (ζ) of the heavy lepton with the standard lepton flavor of 1% yields a decay length $c\tau$ of $\mathcal{O}(1\ \mathrm{nm})$; this implies that, by looking at decays of the heavy lepton within the central detector volume, we remain sensitive down to very small mixing angles. The present upper limit on the mixing parameter squared ζ^2 is ~ 0.005 [6].

Furthermore, we limit ourselves to the case where N and $\mathrm{L}^\pm$ decay via the CC channel only which should be the dominant one since the mass region that we are looking for is near M_W. This can be clearly seen from figure 1. The $\mathrm{W}^{\pm *}$ can decay[1] either hadronically or leptonically. For N production the absence of neutrinos in the CC decay channel allows mass reconstruction, while for $\mathrm{L}^\pm$ production the search in the NC decay channel would be more appropriate for mass reconstruction.

[1] It should be understood that the process is in fact a 3-body decay of the heavy lepton since the W is virtual; however for a heavy lepton mass near M_W, there is also an on-shell component (i.e. a 2-body decay), which is properly taken into account.

We do not study single production of neutral or charged heavy leptons in this analysis, since the production cross sections for $\mathrm{e^+e^-} \to \bar{\nu}_\mathrm{e}\mathrm{N} + \nu_\mathrm{e}\bar{\mathrm{N}}$ and $\mathrm{e^+e^-} \to \mathrm{e^\pm L^\mp}$ are ζ^2 dependent which leads to small cross sections. With the current integrated luminosity, the study of this process is not appropriate.

In this search three different analyses are performed:

(A) $\mathrm{e^+e^-} \to \mathrm{N\bar{N}}$ (neutral heavy lepton), where $\mathrm{N} \to \mathrm{e\,W^*}$, $\mathrm{N} \to \mu\,\mathrm{W^*}$, or $\mathrm{N} \to \tau\,\mathrm{W^*}$. For a Dirac and a Majorana ($\mathrm{N} = \bar{\mathrm{N}}$) type neutral heavy lepton we have that:

<u>Dirac</u>

$$
\begin{array}{l}
\mathrm{e^+e^-} \longrightarrow \mathrm{N\,\bar{N}}\\
\quad \hookrightarrow \ell^+ \mathrm{W}^{-*}\\
\qquad \hookrightarrow \mathrm{q_i\bar{q}_j}\,,\ \ell^-\bar{\nu}_\ell\\
\quad \hookrightarrow \ell^- \mathrm{W}^{+*}\\
\qquad \hookrightarrow \mathrm{q_k}\bar{\mathrm{q}}_\ell\,,\ \ell^+\nu_\ell
\end{array}
$$

<u>Majorana</u>

$$
\begin{array}{l}
\mathrm{e^+e^-} \longrightarrow \mathrm{N\,\bar{N}}\\
\quad \hookrightarrow \ell^\pm \mathrm{W}^{\mp*}\\
\qquad \hookrightarrow \mathrm{q_i\bar{q}_j}\,,\ \ell^\mp\overset{(-)}{\nu}_\ell\\
\quad \hookrightarrow \ell^\pm \mathrm{W}^{\mp*}\\
\qquad \hookrightarrow \mathrm{q_k}\bar{\mathrm{q}}_\ell\,,\ \ell^\mp\overset{(-)}{\nu}_\ell
\end{array}
$$

The typical signature of such an event is at least two isolated charged leptons plus jets. The production cross sections for a Dirac and a Majorana type neutral heavy lepton are shown in figure 2 for various masses (m_N); the curves correspond to $\sqrt{s} = 172$ GeV.

(B) $\mathrm{e^+e^-} \to \mathrm{L^+L^-}$ (charged heavy lepton) where $\mathrm{L^-} \to \nu_\ell \mathrm{W}^{-*}$:

$$
\begin{array}{l}
\mathrm{e^+e^-} \longrightarrow \mathrm{L^+\,L^-}\\
\quad \hookrightarrow \nu_\ell \mathrm{W}^{-*}\\
\qquad \hookrightarrow \mathrm{q_i\bar{q}_j}\,,\ \ell^-\bar{\nu}_\ell\\
\quad \hookrightarrow \bar{\nu}_\ell \mathrm{W}^{+*}\\
\qquad \hookrightarrow \mathrm{q_k}\bar{\mathrm{q}}_\ell\,,\ \ell^+\nu_\ell
\end{array}
$$

This process leads typically to multijet events with large transverse momentum or transverse missing energy. The production cross section for charged heavy lepton pairs is shown in figure 3 for various masses (m_L); the curve corresponds to $\sqrt{s} = 172$ GeV.

(C) $\mathrm{e^+e^-} \to \mathrm{L^+L^-}$ (charged heavy lepton) where $\mathrm{L^-} \to \mathrm{N\,W}^{-*}$ (where N is a stable neutral heavy lepton which decays outside the detector). This production is possible if N is a lighter member of an SU(2) doublet.

$$
\begin{array}{l}
\mathrm{e^+e^-} \longrightarrow \mathrm{L^+\,L^-}\\
\quad \hookrightarrow \mathrm{N\,W}^{-*}\\
\qquad \hookrightarrow \mathrm{q_i\bar{q}_j}\,,\ \ell^-\bar{\nu}_\ell\\
\quad \hookrightarrow \bar{\mathrm{N}}\,\mathrm{W}^{+*}\\
\qquad \hookrightarrow \mathrm{q_k}\bar{\mathrm{q}}_\ell\,,\ \ell^+\nu_\ell
\end{array}
$$

This signal leads to a very low visible energy if the mass difference $m_\mathrm{L} - m_\mathrm{N}$ is small.

We do not study here the cascade decay process in which $L^- \to N\,W^{-*}$ and where N decays into ℓW^* within the OPAL detector volume. This process leads to a complicated topology:

$$
\begin{array}{l}
e^+e^- \longrightarrow L^+ L^- \\
\qquad \hookrightarrow N\,W^{-*} \\
\qquad\qquad \hookrightarrow q_i\bar{q}_j\,,\ \ell^-\bar{\nu}_\ell \\
\qquad\qquad \hookrightarrow \ell^- W^{+*} \\
\qquad\qquad\qquad \hookrightarrow q_k\bar{q}_\ell\,,\ \ell^+\nu_\ell \\
\qquad \hookrightarrow \bar{N}\,W^{+*} \\
\qquad\qquad \hookrightarrow q_k\bar{q}_\ell\,,\ \ell^+\nu_\ell \\
\qquad\qquad \hookrightarrow \ell^+ W^{-*} \\
\qquad\qquad\qquad \hookrightarrow q_i\bar{q}_j\,,\ \ell^-\bar{\nu}_\ell
\end{array}
$$

The following sections present a brief description of the OPAL detector, the Monte Carlo simulation of signal and background events, the analysis flow for each case and finally the results obtained.

2 The OPAL Detector

The OPAL detector is fully described elsewhere [7]. The main sub-detectors which are relevant to our study are: the central detector which consists of a system of tracking chambers providing charged particle tracking over 96% of the full solid angle[2] inside a 0.435 T solenoidal magnetic field; it also allows for particle identification by means of dE/dx sampling. The magnetic coil is surrounded by a lead-glass electromagnetic calorimeter covering the full azimuthal range with excellent hermiticity in the polar angle range of $|\cos\theta| < 0.82$ for the barrel region and $0.81 < |\cos\theta| < 0.984$ for the endcap region. The magnet return yoke is instrumented for hadron calorimetry consisting of barrel and endcap sections along with pole tips that together cover the region $|\cos\theta| < 0.99$. Four layers of muon chambers cover the outside of the hadron calorimeter. Electromagnetic calorimeters close to the beam axis complete the geometrical acceptance down to $\theta = 24$ mrad. These include the forward detectors which are lead-scintillator sandwich calorimeters and, at very small angles, silicon tungsten calorimeters [8] located at both sides of the interaction point. The gap between the endcap electromagnetic calorimeter and the forward detector is instrumented with an additional lead-scintillator electromagnetic calorimeter, called the gamma-catcher.

3 Monte Carlo Simulation

Although a whole range of heavy lepton masses are possible, the analysis will be limited to mass regions not already excluded at LEP and kinematically allowed by the total available energy. A new Monte Carlo generator, EXOTIC [9], has been used for the simulation of $e^+e^- \to N\bar{N}$

[2]The coordinate system adopted by OPAL is that the z axis is the direction of the electron beam, the x axis is horizontal and points towards the center of the LEP ring and the y axis is vertical.

and $e^+e^- \to L^+L^-$ events. The code is based on formulae given in references [5, 10] and the matrix elements include all spin correlations in the production and decay processes of the heavy leptons; it uses JETSET [11] for fragmentation and hadronization of quarks. For $N\bar{N}$ (Dirac type) production, Monte Carlo samples with N having a mass in the range of 70 to 80 GeV have been simulated for the cases $N \to e^-W^{+*}$ and $N \to \mu^-W^{+*}$ (2000 events for each sample); while for the case $N \to \tau^-W^{+*}$ the masses are in the range of 65 to 80 GeV. For $N\bar{N}$ (Majorana type) different Monte Carlo samples were generated taking into account the fact that a Majorana neutral heavy lepton has a different $\cos\theta$ distribution, which is symmetric (θ is the scattering angle of N with respect to the electron beam direction). The $\cos\theta$ distributions for various types of neutral heavy leptons are shown in figure 4. The Majorana type Monte Carlo samples are generated using masses ranging from 60 to 75 GeV for $N \to e^\pm W^{\mp*}$ and $N \to \mu^\pm W^{\mp*}$, and from 55 to 75 GeV for $N \to \tau^\pm W^{\mp*}$. For L^+L^- production where $L^- \to \nu_\ell W^{-*}$, the events were generated with a mass of 75 and 80 GeV (2000 events for each sample). For the case where $L^- \to N\,W^{-*}$, events were simulated at 30 points in the (m_L,m_N) plane, with m_L ranging from 70 to 85 GeV and m_N from 40 to 80 GeV (with 1000 events for each sample), and with a mass difference $m_L - m_N$ larger than 5 GeV. The choice of the masses for the Monte Carlo samples is suggested by the present limits on m_N and m_L.

Various potential backgrounds were also simulated. Below is a list of the most important ones relevant to these searches and ordered by relative importance of cross section:

- two-photon process: in the low Q^2 region ($Q^2 < 1$ GeV^2) with $M_{\gamma\gamma} > 2$ GeV, the PHOJET [12] generator was used (19.88 nb). For the high Q^2 region ($Q^2 > 1$ GeV^2) with $M^2_{\gamma\gamma} > 3$ GeV^2 the PYTHIA [11] generator was used (722.54 pb). The region $Q^2 < 1$ GeV^2 with $M_{\gamma\gamma} < 2$ GeV has not been simulated (this region does not represent a serious background to this analysis). For the leptonic mode ($e^+e^-\tau^+\tau^-$) the Vermaseren generator [13] was used (410 pb).
- multihadronic events ($e^+e^- \to q\,\bar{q}(\gamma)$), simulated with PYTHIA [11] (122.7 pb).
- W^+W^- pairs production simulated with PYTHIA [11] (11.52 pb).
- τ pairs ($e^+e^- \to \tau^+\tau^-(\gamma)$), simulated with KORALZ [14] (10.7 pb).
- neutral current 4-fermion processes, simulated with FERMISV [15] (9.44 pb).

All Monte Carlo events were processed through a full simulation [16] of the OPAL detector, and the same analysis flow is applied to the data sample and the Monte Carlo samples.

4 Data Analysis and candidate selection

We present here the procedure applied for each of the cases described above. The central tracking detector and the electromagnetic calorimeter were required to be fully operational. All charged tracks and calorimeter clusters are subjected to some quality criteria: (i) each track is required to have a minimum transverse momentum (p_T) of 0.15 GeV, to have a minimum number of 20 hits in the central tracking detector, and to point to the geometrical center of the detector within 2 cm and to pass within 25 cm in z at the point of closest approach in $r\phi$; (ii) each electromagnetic cluster in the barrel is required to have a minimum raw energy of 0.1

GeV, while for the endcap regions the minimum raw energy is 0.25 GeV ; (iii) hadronic clusters are required to have a minimum energy of 0.25 GeV. The event visible momentum four-vector is computed from all tracks and clusters and by making a correction which takes into account their possible association [19]; the missing momentum four-vector is extracted from the visible momentum vector. Jet reconstruction is done by using the $k_{\perp}$ ("Durham") [18] jet-finding algorithm with a resolution parameter y_{cut} of 0.004. For electron, muon, and tau identification the following procedures were applied:

electron candidates: a track was identified as an electron candidate if at least one of the following two methods was satisfied:

- method(1): a standard electron identification: each good charged track in the central detector, which satisfies all the following criteria, is considered as an electron candidate:
  - $p > 3.0$ GeV, where p is the track momentum.
  - $0.7 < E/p < 1.4$, where E is the energy of the electromagnetic cluster associated to the track.
  - $8 < dE/dx < 13$ (keV/cm), where dE/dx is the energy loss measured in the central detector.
  - the number of dE/dx measurements is at least 20.
- method (2): the response of an artificial neural net designed to identify electrons [17] was required to exceed 0.95. The net uses information as input mainly from the track momentum, the specific ionization loss, the energy in the associated electromagnetic calorimeter cluster, the number of lead-glass blocks in the cluster, and the presampler signal associated with the track.

In each case there is an isolation requirement on the electron candidate using the total energy in a cone of half opening angle of 15° surrounding the electron, excluding the energy of the electromagnetic cluster associated with the identified candidate. The electron is considered to be isolated if this energy does not exceed 5 GeV.

muon candidates: a track with $p > 3.0$ GeV was identified as a muon candidate if it matched with track segments in a muon chamber. In regions not covered by the muon chambers the identification is done by using a match with the hadron calorimeter strips. We require that muon candidates be isolated as described above for electrons.

tau candidates: a τ candidate was selected by either the electron or muon identification (as above) for a 1-prong tau decay into an isolated lepton (e or μ), or by jet reconstruction for a 1-prong or a 3-prong tau decay into hadrons. A jet was identified as a tau if either of the following criteria were satisfied:

- for 1-prong decay:
  - it contained at least 1 track with $p > 3.0$ GeV.
  - no track was found within a cone of half opening angle of 15° surrounding the highest momentum track.

- the momentum sum of the other tracks within the jet was less than 1.0 GeV.
- the invariant mass of all tracks and clusters within the cone was less than 3.0 GeV.

- for 3-prong decay:
  - it contained exactly 3 tracks in a cone of half opening angle of 15°.
  - the momentum sum of the 3 tracks is greater than 3.0 GeV.
  - the invariant mass of all tracks and clusters within the cone was less than 3.0 GeV.

4.1 Case A: selection of $\mathrm{N\bar{N}}$ candidates

In order to be considered as potential $\mathrm{N\bar{N}}$ candidates, the events must pass the following set of cuts:

(A1) A standard multihadronic selection where tracks and energy clusters satisfy the following:

- $R_{\mathrm{vis}} \geq 0.10$, where $R_{\mathrm{vis}} = \frac{E_{\mathrm{shw}}}{2\times E_{\mathrm{beam}}}$; $E_{\mathrm{shw}} = \sum E_{\mathrm{raw}}$ and E_{raw} is the raw energy of a good cluster.
- $R_{\mathrm{bal}} \leq 0.65$, where $R_{\mathrm{bal}} = \frac{E_{\mathrm{bal}}}{E_{\mathrm{shw}}}$; $E_{\mathrm{bal}} = \sum E_{\mathrm{raw}} \cos\theta$ (θ is the polar angle of the cluster).
- There are at least 7 good clusters.
- There are at least 5 good tracks.

(A2) There are at least 2 isolated leptons of the same flavor (e^-, μ^-, or τ^-). We do not apply a charge constraint in order to be sensitive to both Dirac and Majorana neutral heavy leptons.

(A3) In order to reject radiative events, i.e. events where the effective center-of-mass energy is lower (typically $\sim M_{\mathrm{Z}}$) due to initial state radiation, we require that $|\cos\theta_{\mathrm{miss}}| < 0.95$, if $E_{\mathrm{miss}} > 35$ GeV, where θ_{miss} is the angle between the missing energy vector and the beam axis. The distributions (after cut (A2)) of $|\cos\theta_{\mathrm{miss}}|$ versus E_{miss} are shown in figure 5.

(A4) The number of reconstructed jets is required to be at least four. The distributions (after cut (A2)) of the number of reconstructed jets are shown in figure 5.

For the cases $\mathrm{N} \to \mathrm{e\,W^*}$ and $\mathrm{N} \to \mu\,\mathrm{W^*}$ the remaining number of events after each cut are displayed in tables 1 and 2 respectively (numbers for Dirac and Majorana type N are displayed on the same table).

For the case $\mathrm{N} \to \tau\,\mathrm{W^*}$ one needs extra cuts as the background is larger:

(A5) For the case $\mathrm{N} \to \tau\,\mathrm{W^*}$ we require in addition that $65 < E_{\mathrm{vis}} < 160$ GeV, where E_{vis} is the visible energy. The visible energy distributions are shown in figure 6.

The number of events remaining in this case after each cut are displayed in table 3.

The efficiencies obtained for the $\mathrm{N\bar{N}}$ selection after applying the cuts mentioned above are evaluated from the Monte Carlo samples and are shown in table 4 for a Dirac and table 5 for a Majorana type neutral heavy lepton.

	data	total bkg	$q\bar{q}(\gamma)$	$\gamma\gamma$	$\tau^+\tau^-$	4-f	Dirac $m_N = 75$	Majorana $m_N = 65$
cut A1	1411	1288	1137	26.6	3.33	120.8	5.67	4.15
cut A2	1	1.72	0.35	0.0	0.03	1.34	4.07	3.14
cut A3	1	1.48	0.21	0.0	0.03	1.25	4.01	3.07
cut A4	0	0.68	0.08	0.0	0.01	0.59	3.88	2.89

Table 1: Observed number of events in the data sample and expected number of events from the background sources and the $N\bar{N}$ signal (Dirac and Majorana types) for the case where $N \to e\,W^*$. The numbers correspond to an integrated luminosity of 10.4 pb^{-1}. The four-fermion (4-f) column includes WW pairs.

	data	total bkg	$q\bar{q}(\gamma)$	$\gamma\gamma$	$\tau^+\tau^-$	4-f	Dirac $m_N = 75$	Majorana $m_N = 65$
cut A1	1411	1288	1137	26.6	3.33	120.8	5.37	3.81
cut A2	0	1.23	0.27	0.0	0.0	0.96	3.41	2.53
cut A3	0	1.02	0.13	0.0	0.0	0.89	3.37	2.47
cut A4	0	0.51	0.04	0.0	0.0	0.47	3.28	2.36

Table 2: Observed number of events in the data sample and expected number of events from the background sources and the $N\bar{N}$ signal (Dirac and Majorana types) for the case where $N \to \mu\,W^*$. The numbers correspond to an integrated luminosity of 10.4 pb^{-1}. The four-fermion (4-f) column includes WW pairs.

4.2 Case B: selection of L^+L^- candidates with $L^- \to \nu_\ell W^{-*}$

In order to be considered as potential L^+L^- candidates, where each charged heavy lepton decays into a light standard neutrino and an off-shell W boson, the events must satisfy the following set of selection criteria:

(B1) The same multihadronic selection as for case A.

(B2) To reduce the background from $q\bar{q}\gamma$ and $\gamma\gamma$ processes we require that the energy deposited in each forward calorimeter (one at each end of the OPAL detector), each gamma-catcher, and each silicon tungsten calorimeter be less that 2 GeV, 5 GeV, and 5 GeV respectively.

(B3) Non-radiative events are selected by demanding that $|\cos\theta_{\rm miss}| < 0.85$. The $|\cos\theta_{\rm miss}|$ distributions after cut (B1) are shown in figure 7-(a).

(B4) In order to reject events containing two back-to-back jets mostly from $q\bar{q}(\gamma)$, the thrust of the event was required to be less than 0.85. The thrust distributions after cut (B1) are shown in figure 7-(b).

	data	total bkg	$q\,\bar{q}(\gamma)$	$\gamma\gamma$	$\tau^+\tau^-$	4-f	Dirac $m_{\mathrm{N}} = 65$	Majorana $m_{\mathrm{N}} = 55$
cut A1	1411	1288	1137	26.6	3.33	120.8	9.42	7.62
cut A2	4	7.99	2.44	0.59	0.10	4.84	3.68	2.86
cut A3	4	6.53	1.41	0.48	0.09	4.52	3.62	2.81
cut A4	3	3.52	0.61	0.48	0.02	2.40	3.26	2.45
cut A5	2	1.98	0.21	0.0	0.01	1.76	3.05	2.26

Table 3: Observed number of events in the data sample and expected number of events from the background sources and the $\mathrm{N}\bar{\mathrm{N}}$ signal (Dirac and Majorana types) for the case where $\mathrm{N} \to \tau\,\mathrm{W}^*$. The numbers correspond to an integrated luminosity of 10.4 pb^{-1}. The four-fermion (4-f) column includes WW pairs.

	Dirac $\mathrm{N} \to \mathrm{e}\,\mathrm{W}^*$	Dirac $\mathrm{N} \to \mu\,\mathrm{W}^*$	Dirac $\mathrm{N} \to \tau\,\mathrm{W}^*$
$m_{\mathrm{N}} = 65$	-	-	30.3 ± 1.0
$m_{\mathrm{N}} = 70$	62.7 ± 1.1	50.0 ± 1.1	27.2 ± 1.0
$m_{\mathrm{N}} = 75$	61.9 ± 1.1	52.2 ± 1.1	27.9 ± 1.0
$m_{\mathrm{N}} = 80$	58.3 ± 1.1	47.8 ± 1.1	21.9 ± 0.9

Table 4: Selection efficiencies (in per cent) for $\mathrm{N}\bar{\mathrm{N}}$ (Dirac type) candidates selection for various masses of N. The errors are statistical.

(B5) If no isolated lepton is found in the event we apply the following constraints:

- $80 < E_{\mathrm{vis}} < 145$ GeV. The distributions of the visible energy after the (B4) are shown in figure 8-(a).
- $p_{\mathrm{Tmiss}} > 15$ GeV, where p_{Tmiss} is the missing transverse momentum or the event transverse momentum. The distributions of p_{Tmiss} after cut (B4) are shown in figure 8-(b).
- $N_{\mathrm{jets}} \geq 4$, where N_{jets} is the number of reconstructed jets. The distributions of the number of reconstructed jets after the (B4) are shown in figure 8-(c).
- the maximum momentum of a good track should not exceed 25 GeV. The maximum track momentum distributions after cut (B4) are shown in figure 8-(d).

(B6) If one or more isolated lepton is found, we apply the following cuts:

- $40 < E_{\mathrm{vis}} < 100$ GeV. The E_{vis} distributions after the cut (B4) are shown in figure 9-(a).
- $p_{\mathrm{Tmiss}} > 20$ GeV. The p_{Tmiss} distributions after cut (B4) are shown in figure 9-(b).

	Majorana $\mathrm{N} \to \mathrm{e\,W}^*$	$\mathrm{N} \to \mu\,\mathrm{W}^*$	$\mathrm{N} \to \tau\,\mathrm{W}^*$
$m_{\mathrm{N}} = 55$	-	-	27.4 ± 1.0
$m_{\mathrm{N}} = 60$	60.9 ± 1.1	48.3 ± 1.1	28.7 ± 1.0
$m_{\mathrm{N}} = 65$	63.0 ± 1.1	51.5 ± 1.1	29.1 ± 1.0
$m_{\mathrm{N}} = 70$	65.6 ± 1.1	52.5 ± 1.1	29.3 ± 1.0
$m_{\mathrm{N}} = 75$	63.6 ± 1.1	51.8 ± 1.1	26.8 ± 1.0

Table 5: Selection efficiencies (in per cent) for $\mathrm{N\bar{N}}$ (Majorana type) candidates selection for various masses of N. The errors are statistical.

- $N_{\mathrm{jets}} \geq 3$. The N_{jets} distributions after cut (B4) are shown in figure 9-(c).

The remaining number of events after each cut are displayed in table 6. The efficiencies obtained after all cuts are shown in table 7.

	data	total bkg	$\mathrm{q\,\bar{q}}(\gamma)$	$\gamma\gamma$	$\tau^+\tau^-$	4-f	$\mathrm{L^+L^-}$ $m_{\mathrm{L}} = 80$
cut B1	1411	1288	1137	26.6	3.33	120.8	12.5
cut B2	1044	990.3	866.5	11.2	2.84	109.9	11.5
cut B3	406	398.8	303.7	3.60	1.71	89.8	10.1
cut B4	133	129.6	70.4	1.65	0.23	57.3	7.4
cut B5 or B6	1	3.07	0.78	0.0	0.01	2.28	3.2

Table 6: Observed number of events in the data sample and expected number of events from the background sources and the $\mathrm{L^+L^-}$ signal for the case where $\mathrm{L^-} \to \nu_\ell \mathrm{W}^{-*}$. The numbers correspond to an integrated luminosity of 10.4 pb^{-1}. The four-fermion (4-f) column includes WW pairs.

4.3 Case C: selection of $\mathrm{L^+L^-}$ candidates with $\mathrm{L^-} \to \mathrm{N\,W}^{-*}$

In order to be considered as potential $\mathrm{L^+L^-}$ candidates, where the charged heavy lepton decays into a stable neutral heavy lepton (within the detector volume) and an off-shell W boson, the events must satisfy the following set of cuts: (here we do not use the standard multihadronic events selection since for small mass differences $m_{\mathrm{L}} - m_{\mathrm{N}}$ the visible energy is very low and particle multiplicity small).

(C1) We require at least 5 good charged tracks.

(C2) To reduce the large background coming from two-photon processes, we apply a cut on

m_{L} (GeV)	efficiency (%)
75	25.9 ± 1.0
80	21.8 ± 0.9

Table 7: Selection efficiencies (in per cent) for $\mathrm{L^+L^-}$ candidates ($\mathrm{L^-} \to \nu_\ell \mathrm{W^{-*}}$). The errors are statistical.

the missing transverse momentum: $p_{\mathrm{Tmiss}} > 12$ GeV. The distributions of p_{Tmiss} are shown in figure 10-(a).

(C3) The criteria for energy deposited in the forward detector, the gamma-catcher, and the silicon tungsten calorimeter are the same as in case B.

(C4) In order to reduce background from beam-gas and beam-wall interactions we require that $|\cos\theta_{\mathrm{thrust}}|$ be smaller than 0.9, where θ_{thrust} is the polar angle of the thrust axis. The $|\cos\theta_{\mathrm{thrust}}|$ distributions are shown in figure 10-(b).

(C5) For radiative event rejection we require that $|\cos\theta_{\mathrm{miss}}| < 0.7$. The $|\cos\theta_{\mathrm{miss}}|$ distributions are shown in figure 10-(c).

(C6) The two heavy neutrinos coming from $\mathrm{L^+}$ and $\mathrm{L^-}$ carry away a significant fraction of the energy. To reduce the background from multihadronic and four-fermion events, we require that $10 < E_{\mathrm{vis}} < 75$ GeV. The distributions of E_{vis} are shown in figure 10-(d).

(C7) Four-fermion processes and $\tau^+\tau^-$ backgrounds were reduced by requiring that the maximum momentum of a good track should not exceed 25 GeV. The distributions of p_{max} are shown in figure 10-(e).

(C8) We require that the thrust value be less than 0.9 in order to reject events containing two back-to-back jets. The thrust distributions are shown in figure 10-(f).

The remaining number of events after each cut are displayed in table 8. The efficiencies obtained after all cuts are shown in table 9.

5 Results and new mass limits

The total number of expected signal events for arbitrary heavy lepton masses is evaluated from the total production cross section, the total integrated luminosity, and the Monte Carlo detection efficiency obtained from the three analyses (namely case A, case B, and case C) for the simulated mass points using a linear interpolation. The systematic errors on the total number of expected events are estimated to be 2% from the integrated luminosity, typically 1.1% from the Monte Carlo statistics, 3.7 % from lepton identification [3] and 2% from linear interpolation. The error on the total cross section is negligible. The systematic errors are considered to be independent and the total systematic error is the quadratic sum of individual errors. The inclusion of the total systematic error in calculating new mass limits was treated as described in the paper of Cousins and Highland [20]: in order to include the systematic

	data	total bkg	$\mathrm{q\,\bar{q}}(\gamma)$	$\gamma\gamma$	$\tau^+\tau^-$	4-f	$\mathrm{L^+L^-}$ $m_\mathrm{L}=75$ $m_\mathrm{N}=60$	$\mathrm{L^+L^-}$ $m_\mathrm{L}=80$ $m_\mathrm{N}=50$
cut C1	23057	20205	1240	18832	9.17	124.5	14.98	12.13
cut C2	439	323.5	238.1	11.14	5.15	69.1	5.92	9.02
cut C3	316	262.8	192.1	2.23	4.54	63.9	5.79	8.67
cut C4	299	249.4	183.3	0.66	4.10	61.4	5.51	8.15
cut C5	154	135.4	84.2	0.22	2.36	48.6	5.14	7.07
cut C6	5	1.53	0.77	0.07	0.37	0.32	5.14	6.94
cut C7	4	1.37	0.75	0.07	0.30	0.25	5.14	6.89
cut C8	1	0.56	0.36	0.0	0.06	0.14	4.79	6.41

Table 8: Observed number of events in the data sample and expected number of events from the background sources and the $\mathrm{L^+L^-}$ signal for the case where $\mathrm{L^-} \rightarrow \mathrm{N\,W^{-*}}$. The numbers correspond to an integrated luminosity of 10.4 pb^{-1}. The four-fermion (4-f) column includes WW pairs. The two-photon ($\gamma\gamma$) column does not include the region $M_{\gamma\gamma} < 2$ GeV with $Q^2 < 1$ GeV^2.

uncertainties into a limit, the number of events that one should expect for a given C.L. is the number expected from a Poisson statistics with a background subtraction (as suggested by the Particle Data Group [2]), plus a correction term which depends on the relative uncertainty. The number of expected events from $\mathrm{N\bar{N}}$ production for various m_N and the 95 % C.L. limit are shown in figure 11 for a Dirac type and in figure 12 for a Majorana type neutral heavy lepton. For $\mathrm{L^+L^-}$ production where $\mathrm{L^-} \rightarrow \nu_\ell \mathrm{W^{-*}}$ the number of expected signal events for various m_L and the 95 % C.L. limit are shown in figure 13. For the case where $\mathrm{L^-} \rightarrow \mathrm{N\,W^{-*}}$ a 2-dimensional interpolation was used in order to get the expected number of events for any point in the $(m_\mathrm{L}, m_\mathrm{N})$ plane. Figure 14 shows the excluded region obtained by combining with the 161 GeV results [3]. The inclusion of the 161 GeV results is done by adding the number of expected events at $\sqrt{s} = 161$ GeV and $\sqrt{s} = 170,\ 172$ GeV.

The limits on the masses obtained using the data at $\sqrt{s} = 170,\ 172$ GeV only, and by combining the results with those obtained at $\sqrt{s} = 161$ GeV are shown in table 10.

6 Summary and Conclusion

A search has been made for pair production of unstable neutral heavy leptons ($\mathrm{N\bar{N}}$) and charged heavy leptons ($\mathrm{L^+L^-}$) for an integrated luminosity of 10.4 pb^{-1} at $\sqrt{s} = 170$ and 172 GeV collected with the OPAL detector at LEP. No evidence was found for either a Dirac or a Majorana type neutral heavy lepton in the search channels $\mathrm{N} \rightarrow \mathrm{e\,W^*}$, $\mathrm{N} \rightarrow \mu\,\mathrm{W^*}$, and $\mathrm{N} \rightarrow \tau\,\mathrm{W^*}$. No evidence was found either for a charged heavy lepton $\mathrm{L^\pm}$ neither in the scenario where $\mathrm{L^-}$ decays into a light standard neutrino and an off-shell W ($\mathrm{L^-} \rightarrow \nu_\ell \mathrm{W^{-*}}$), nor in the scenario where it decays into a stable neutral heavy lepton, within the OPAL detector volume, and an

	m_{L} (GeV)			
m_{N} (GeV)	70	75	80	85
80	-	-	-	0.0 ± 0.0
75	-	-	0.1 ± 0.1	5.9 ± 0.7
70	-	0.1 ± 0.1	5.7 ± 0.7	23.8 ± 1.3
65	0.1 ± 0.1	8.2 ± 0.9	23.6 ± 1.3	35.2 ± 1.5
60	7.8 ± 0.8	22.3 ± 1.4	35.7 ± 1.5	44.3 ± 1.6
55	24.2 ± 1.3	32.5 ± 1.5	40.3 ± 1.5	47.9 ± 1.6
50	33.2 ± 1.5	41.2 ± 1.5	43.6 ± 1.6	46.8 ± 1.6
45	36.5 ± 1.5	39.3 ± 1.5	40.9 ± 1.5	42.2 ± 1.6
40	35.2 ± 1.5	34.5 ± 1.5	33.0 ± 1.5	31.4 ± 1.5

Table 9: Selection efficiencies (in per cent) for $\mathrm{L}^+\mathrm{L}^-$ candidates in the case where $\mathrm{L}^- \to \mathrm{N\,W}^{-*}$ for various (m_{L},m_{N}) points. The errors are statistical.

off-shell W ($\mathrm{L}^- \to \mathrm{N\,W}^{-*}$).

For $\mathrm{N\bar{N}}$ (Dirac) production we have set the mass limits for m_{N} at 95 % C.L. to be 79.1, 78.5, and 69.0 GeV respectively for the search channels $\mathrm{N} \to \mathrm{e\,W}^*$, $\mathrm{N} \to \mu\,\mathrm{W}^*$, and $\mathrm{N} \to \tau\,\mathrm{W}^*$. For the Majorana case the limits obtained are 69.8 and 68.7 respectively for $\mathrm{N} \to \mathrm{e\,W}^*$ and $\mathrm{N} \to \mu\,\mathrm{W}^*$; the limit can not be improved for the case $\mathrm{N} \to \tau\,\mathrm{W}^*$. These limits are obtained by combining with the results from the analysis done at $\sqrt{s} = 161$ GeV.

For $\mathrm{L}^+\mathrm{L}^-$ production we have set a lower mass limit of 81.4 GeV for the case $\mathrm{L}^- \to \mathrm{N\,W}^{-*}$, with $m_{\mathrm{N}} < 63.9$ GeV (N stable within the detector volume) and a lower limit of 80.2 GeV for the case $\mathrm{L}^- \to \nu_\ell \mathrm{W}^{-*}$, both at 95 % C.L. . These limits are obtained by combining with the results from the analysis done at $\sqrt{s} = 161$ GeV.

References

[1] A. Djouadi, D. Schaile, C. Verzegnassi, et *al.*, Report of the Working Group "Extended Gauge Models" in Proceedings of the workshop "$\mathrm{e}^+\mathrm{e}^-$ Collisions at 500 GeV: the physics potential", P. Zerwas, (ed.) Report DESY 92-123A+B.

[2] L. Montanet *et al.*, Phys. Rev. **D54**, (1996).

[3] OPAL Collaboration, K. Ackerstaff *et al.*, CERN-PPE/96-140.

[4] M. Turner, Physica Scripta **T36** (1991) 167;
M. Sher and Y. Yuan Phys. Lett. **B285** (1992) 336.

[5] A. Djouadi, Z. Phys. **C63** (1994) 317; and references therein.

[6] E. Nardi, E. Roulet, D. Tommasini, Phys. Lett. **B 344** (1995) 225.

		$\sqrt{s} = 170$ and 172 GeV	$\sqrt{s} = 161$, 170, and 172 GeV
$\mathrm{N} \to \mathrm{e\,W}^*$	Dirac	77.8 GeV	79.1 GeV
	Majorana	64.4 GeV	69.8 GeV
$\mathrm{N} \to \mu\,\mathrm{W}^*$	Dirac	75.9 GeV	78.5 GeV
	Majorana	60.4 GeV	68.7 GeV
$\mathrm{N} \to \tau\,\mathrm{W}^*$	Dirac	-	69.0 GeV
	Majorana	-	-
$\mathrm{L}^- \to \nu_\ell \mathrm{W}^{-*}$		79.1 GeV	80.2 GeV
$\mathrm{L}^- \to \mathrm{N\,W}^{-*}$		80.8 GeV (with $m_{\mathrm{N}} < 62.6$)	81.4 GeV (with $m_{\mathrm{N}} < 63.9$)

Table 10: New mass limits obtained with the data collected at 170 and 172 GeV center-of-mass energies (first column) and combined with the results of the 161 GeV data analysis (second column).

[7] OPAL Collaboration, K. Ahmet *et al.*, Nucl. Instr. Meth. **A305** (1991) 275.

[8] B.E. Anderson *et al.*, IEEE Transactions on Nuclear Science **41** (1994) 845.

[9] OPAL Technical Note **TN463**, "EXOTIC 1.0, *A Heavy Fermion and Excited Fermion Monte Carlo Generator for* $\mathrm{e}^+\mathrm{e}^-$ *Physics*".

[10] J.H. Kühn, A. Reiter, and P.M. Zerwas Nucl. Phys. **B 272** (1986) 560.

[11] T. Sjöstrand, Comp. Phys. Comm. **82** (1994) 74.

[12] R. Engel and J. Ranft, ENSLAPP-A-540/95 (1995), and Siegen SI 95-08 (1995).

[13] J. A. M. Vermaseren, Nucl. Phys. **B229** (1983) 347.

[14] S. Jadach, B. F. L. Ward, Z. Wąs, Comp. Phys. Comm. **79** (1994) 503.

[15] J. Hilgart, R.Kleiss, and F. Le Diberder, Comp. Phys. Comm.**75** (1993) 191.

[16] J. Allison *et al.*, Nucl. Instr. Meth. **A317** (1992) 47.

[17] OPAL Technical Note, **TN-317**, "Update of the Neural Net Electron ID".

[18] S. Catani *et al.*, Nucl. Phys. **B269** (1991) 432.

[19] OPAL Technical Note, **TN-306** "GCE++, An Algorithm for Event Energy Measurement".

[20] R.D. Cousins and V.L. Highland, Nucl. Instr. Meth. **A320** (1992) 331.

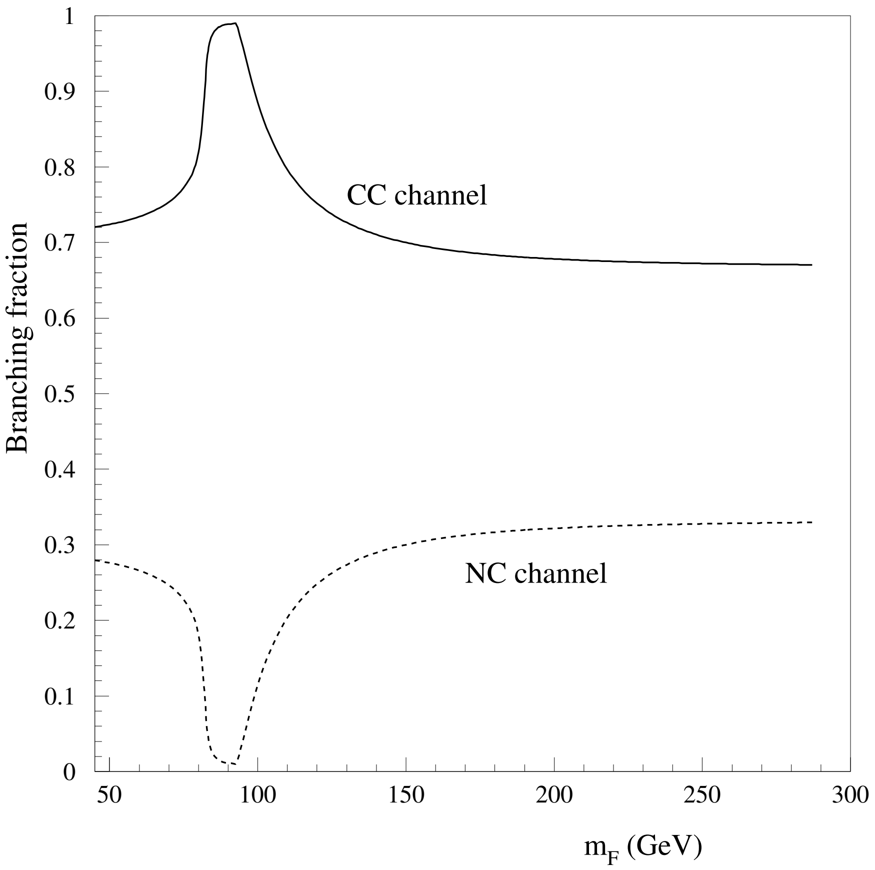

Figure 1: Branching fractions of the decay into the CC channel (solid line) and the NC channel (broken line) of various heavy lepton masses m_{F} as given by EXOTIC [9].

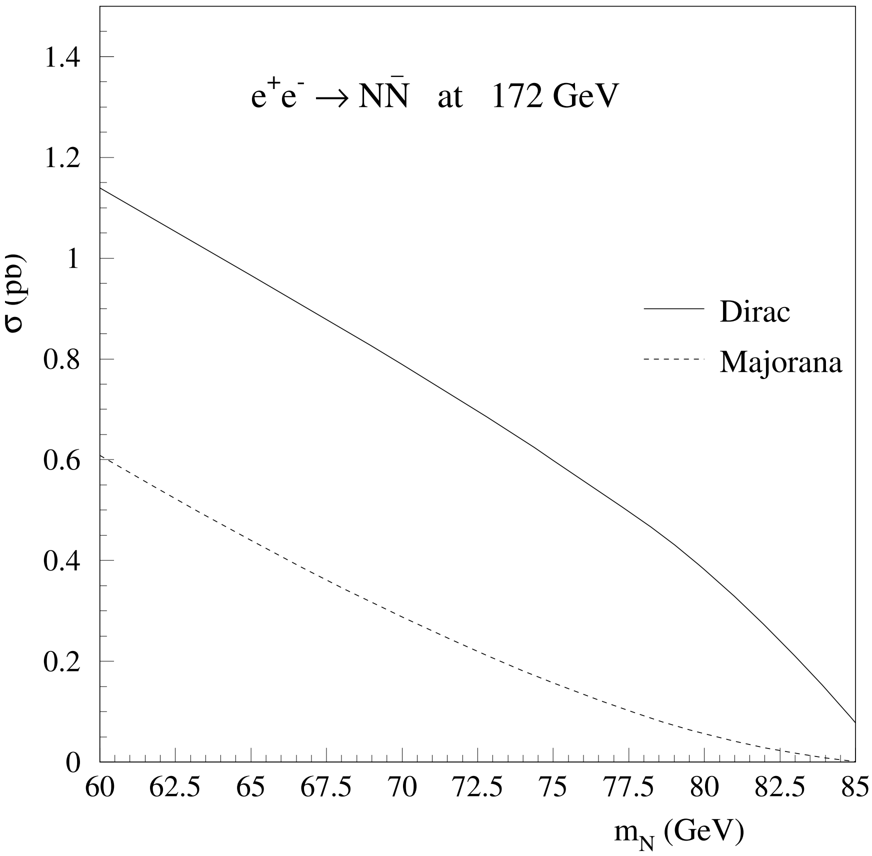

Figure 2: Neutral heavy lepton pairs production cross sections for various masses $m_{\rm N}$ at 172 GeV as given by EXOTIC [9].

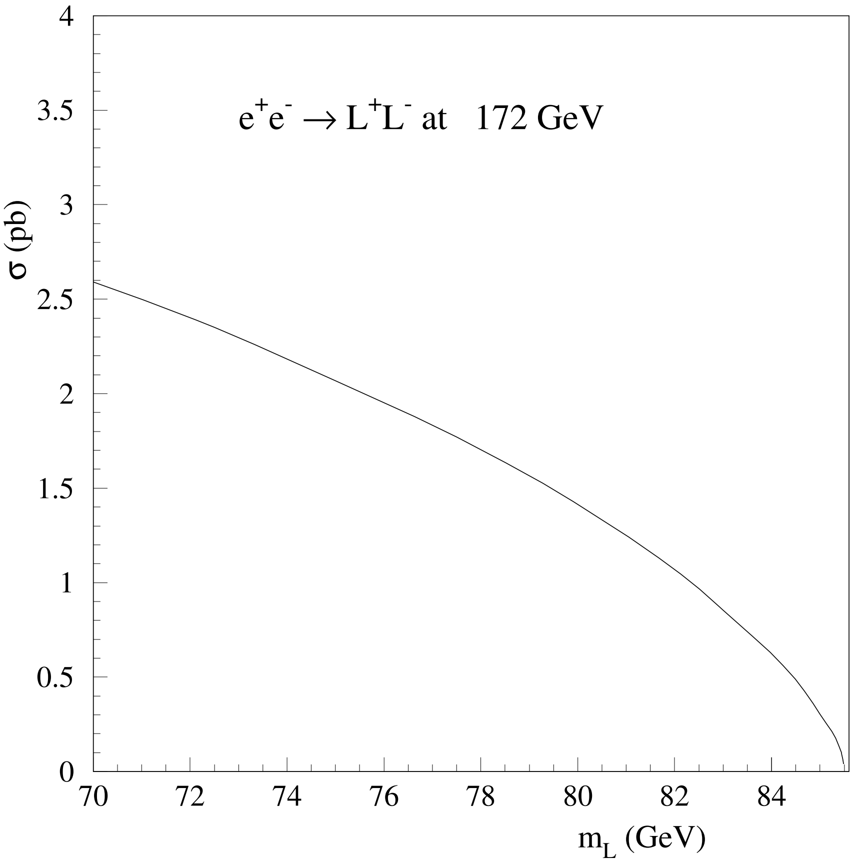

Figure 3: Charged heavy lepton pairs production cross sections for various masses m_{L} at 172 GeV as given by EXOTIC [9].

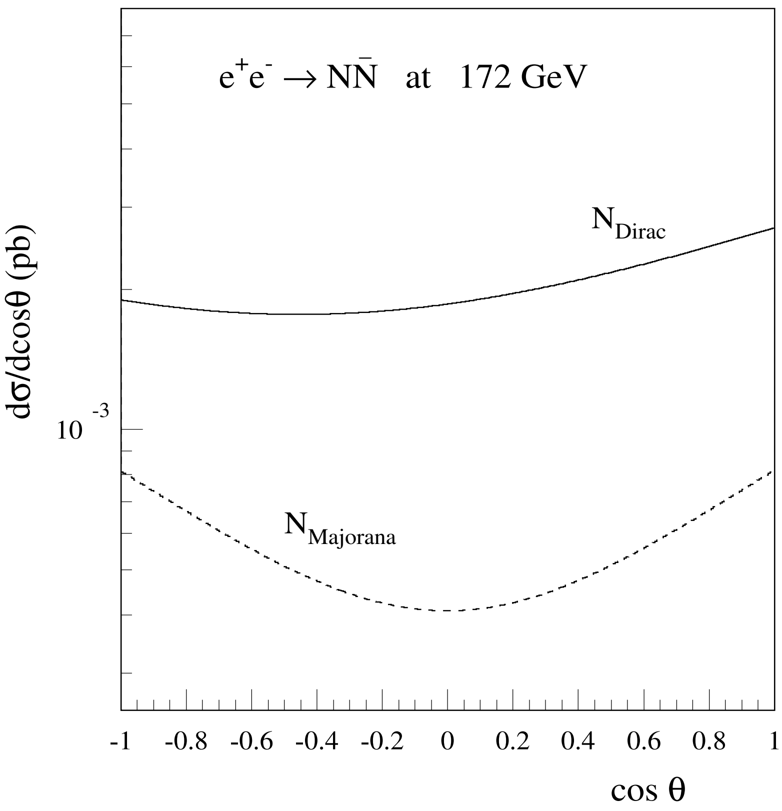

Figure 4: The $\cos\theta$ distributions for $\mathrm{N\bar{N}}$ production at 172 GeV with $m_{\mathrm{N}} = 75$ GeV for a Dirac and a Majorana type N, as given by EXOTIC [9].

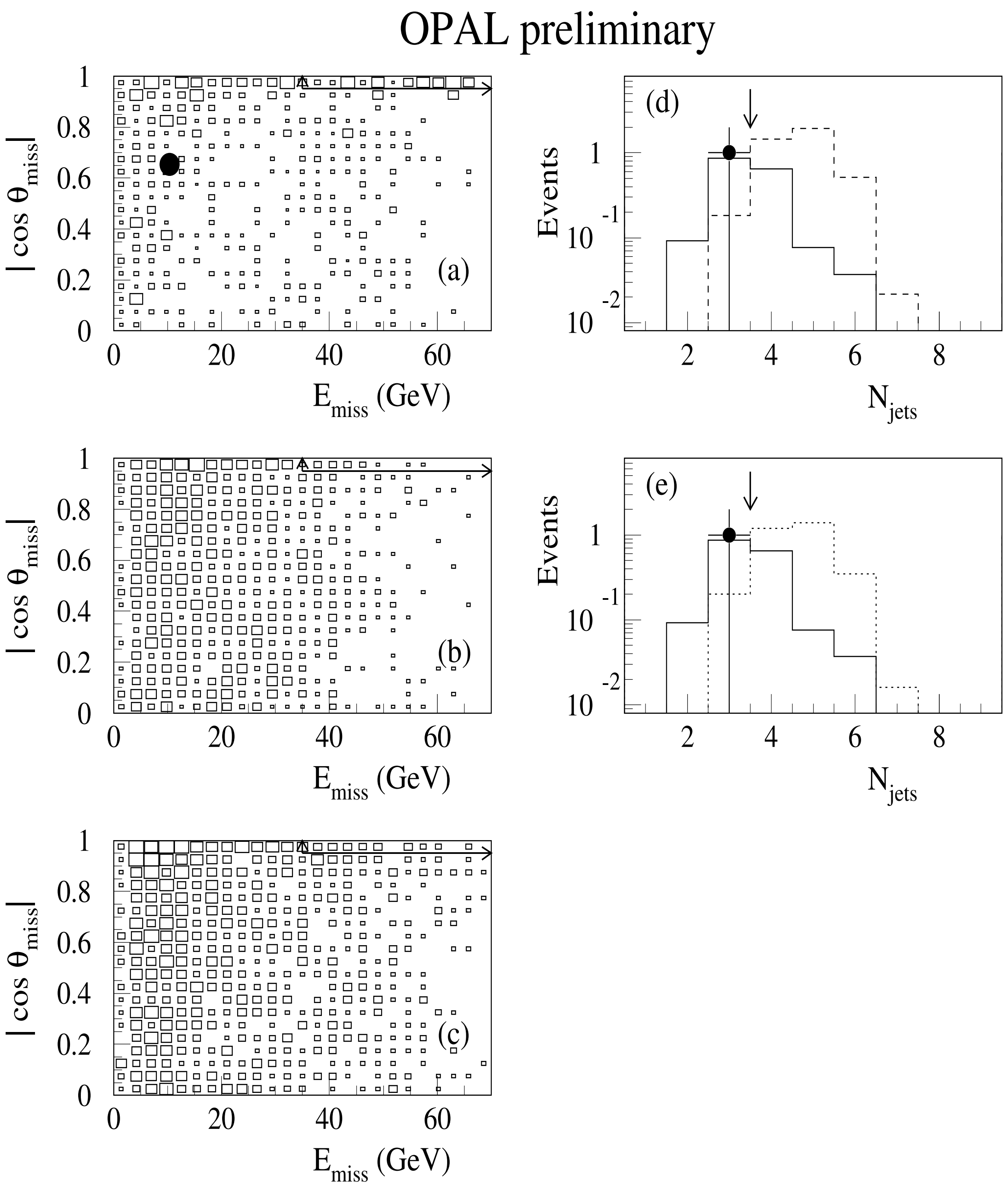

Figure 5: The distributions of $\cos\theta_{\mathrm{miss}}$ versus E_{miss} are shown in (a) for the background processes (box) and the selected event among the data (filled circle) after cut (A2); the distribution for the $\mathrm{N\bar{N}}$ signal with $\mathrm{N} \to \mathrm{e\,W^*}$ is shown in (b) for a Dirac N (with $m_{\mathrm{N}} = 75$ GeV), and in (c) for a Majorana N (with $m_{\mathrm{N}} = 65$ GeV). The distributions for the number of reconstructed jets after cut (A2) are shown in (d) for the data (point), the background processes (solid line), and the $\mathrm{N\bar{N}}$ signal (Dirac N, with $\mathrm{N} \to \mathrm{e\,W^*}$) for the case where $m_{\mathrm{N}} = 75$ GeV (broken line); the corresponding distribution for a Majorana N (with $m_{\mathrm{N}} = 65$ GeV) is shown in (e) (dotted line). The arrows correspond to the cut values.

OPAL preliminary

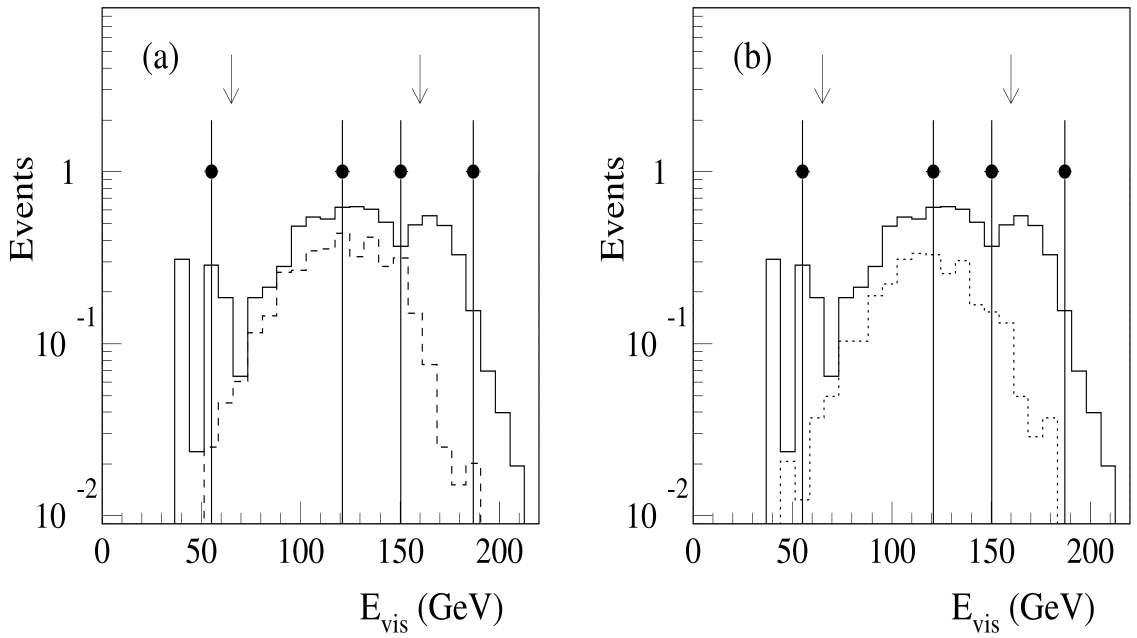

Figure 6: The visible energy (E_{vis}) distributions after cut (A2) are shown in (a) for the data (points), the background processes (solid line), and the $\mathrm{N}\bar{\mathrm{N}}$ signal with $\mathrm{N} \to \tau\,\mathrm{W}^*$ (Dirac N, with $m_{\mathrm{N}} = 65$ GeV); the corresponding distribution for a Majorana N (with $m_{\mathrm{N}} = 55$ GeV) is shown in (b) (dotted line). The arrows correspond to the cut values.

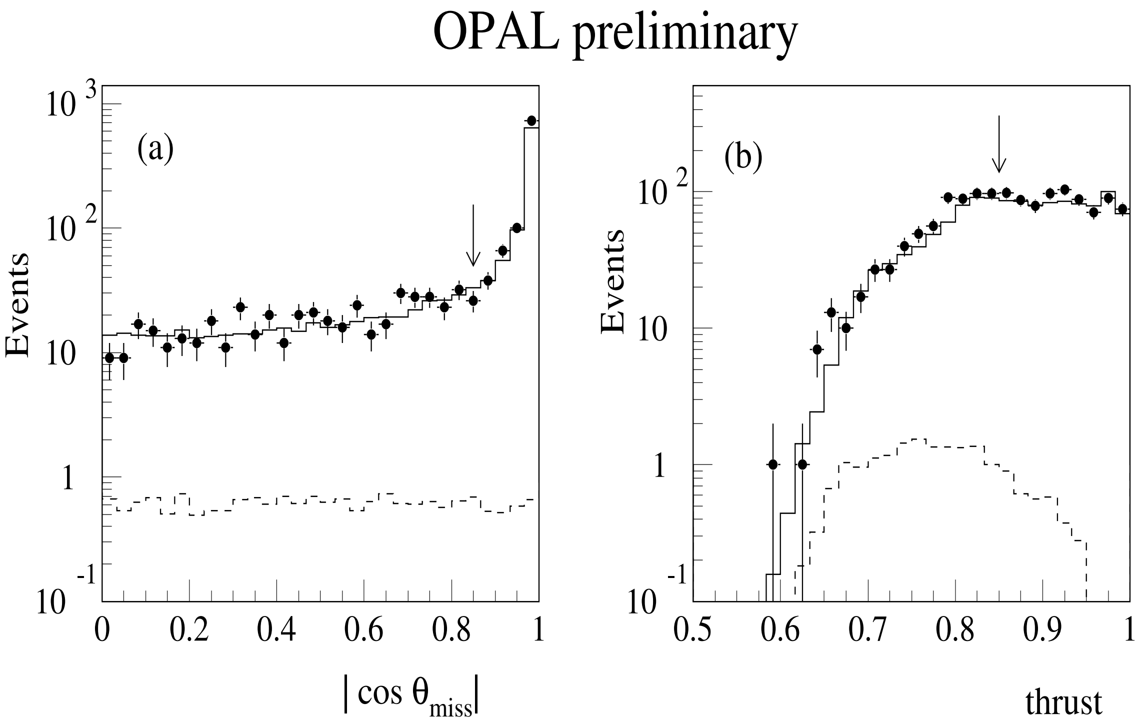

Figure 7: The plots show the distributions after cut (B1) for the data (points), the background processes (solid line), and the L^+L^- signal with $L^- \to \nu_\ell W^{-*}$ for the case where $m_L = 75$ GeV (broken line) respectively for $\cos\theta_{miss}$ (a) and thrust (b). The arrows correspond to the cut values.

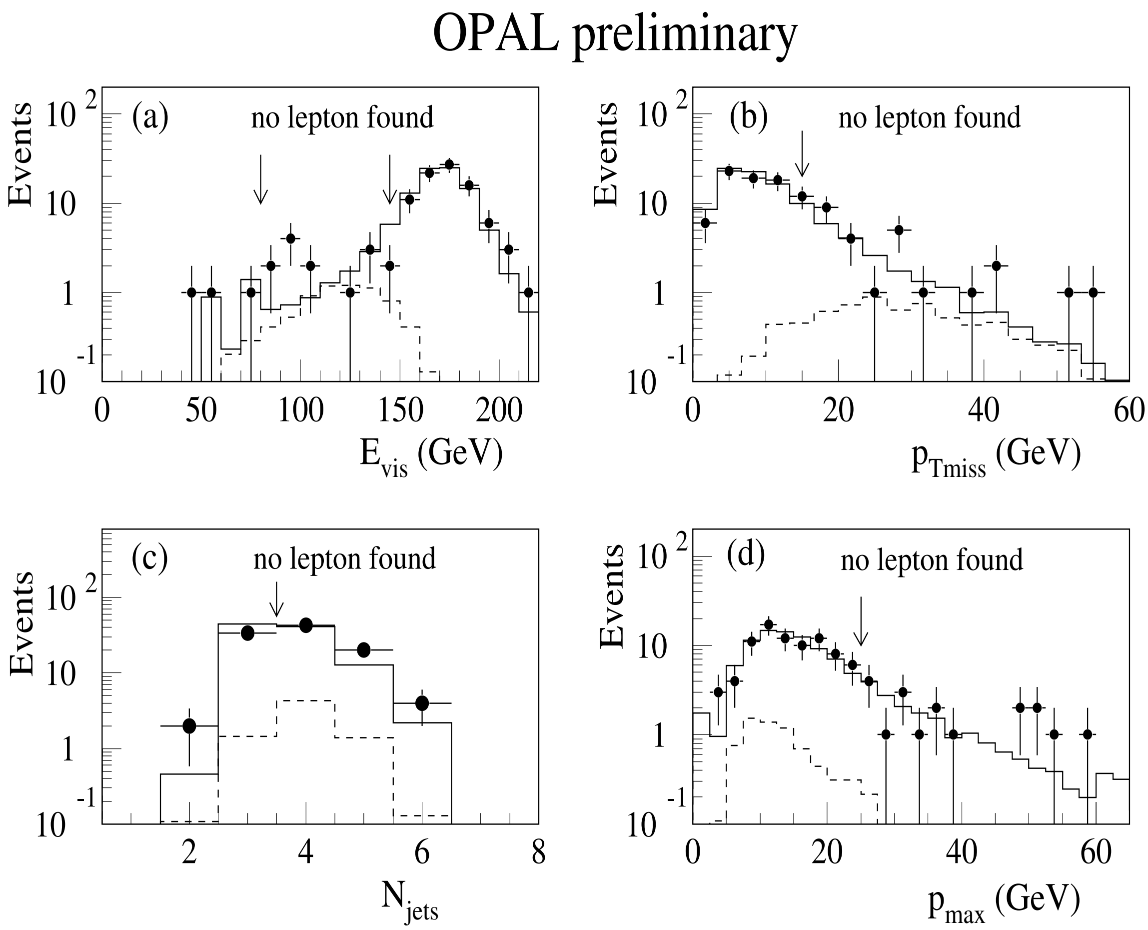

Figure 8: The plots show the distributions after cut (B4), in the case where no isolated lepton is found, for the data (points), the background processes (solid line), and the L^+L^- signal with $L^- \to \nu_\ell W^{-*}$ for the case $m_L = 75$ GeV (broken line) respectively for the visible energy (a), the missing transverse momentum (b), the number of reconstructed jets (c), and the maximum track momentum (d). The arrows correspond to the cut values.

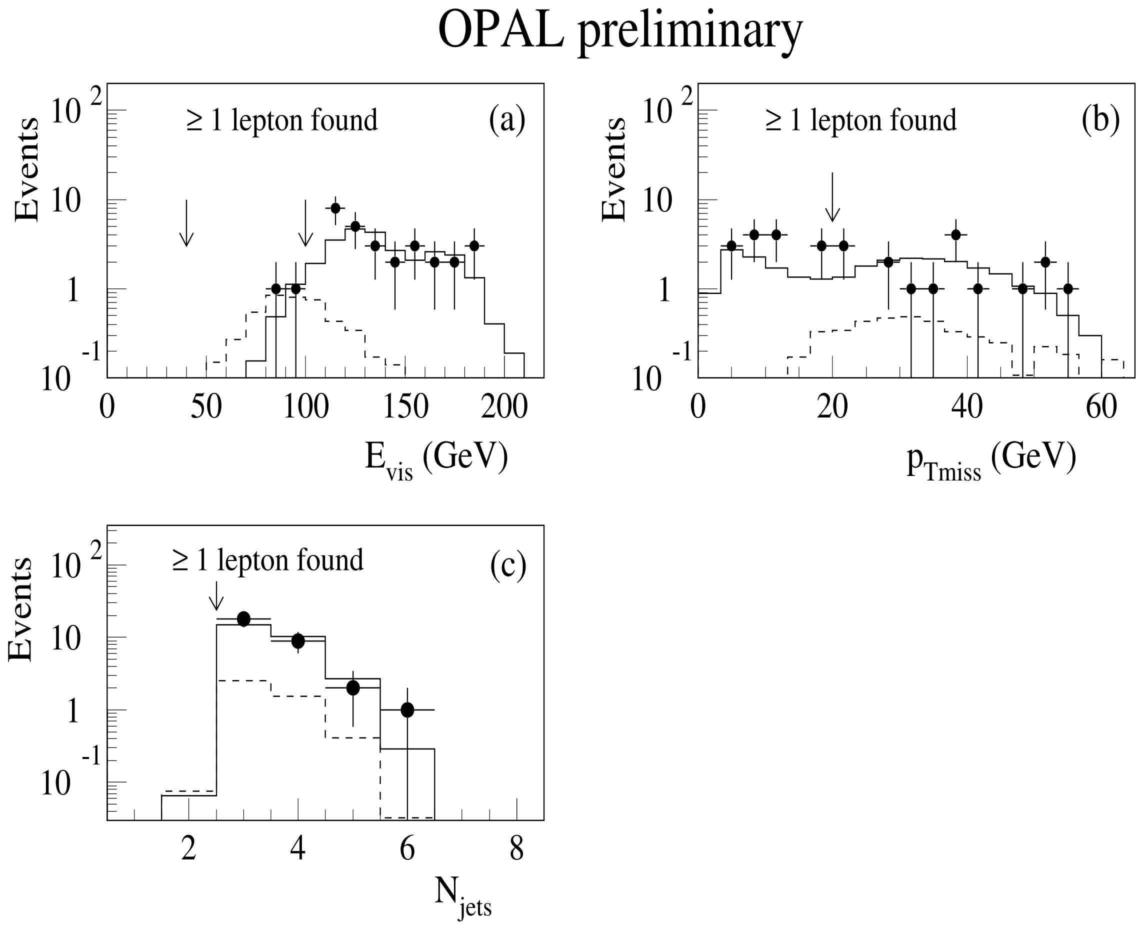

Figure 9: The plots show the distributions after cut (B4), in the case where at least one isolated lepton is found, for the data (points), the background processes (solid line), and the L^+L^- signal with $L^- \to \nu_\ell W^{-*}$ for the case $m_L = 75$ GeV (broken line) respectively for the visible energy (a), the missing transverse momentum (b), and the number of reconstructed jets (c). The arrows correspond to the cut values.

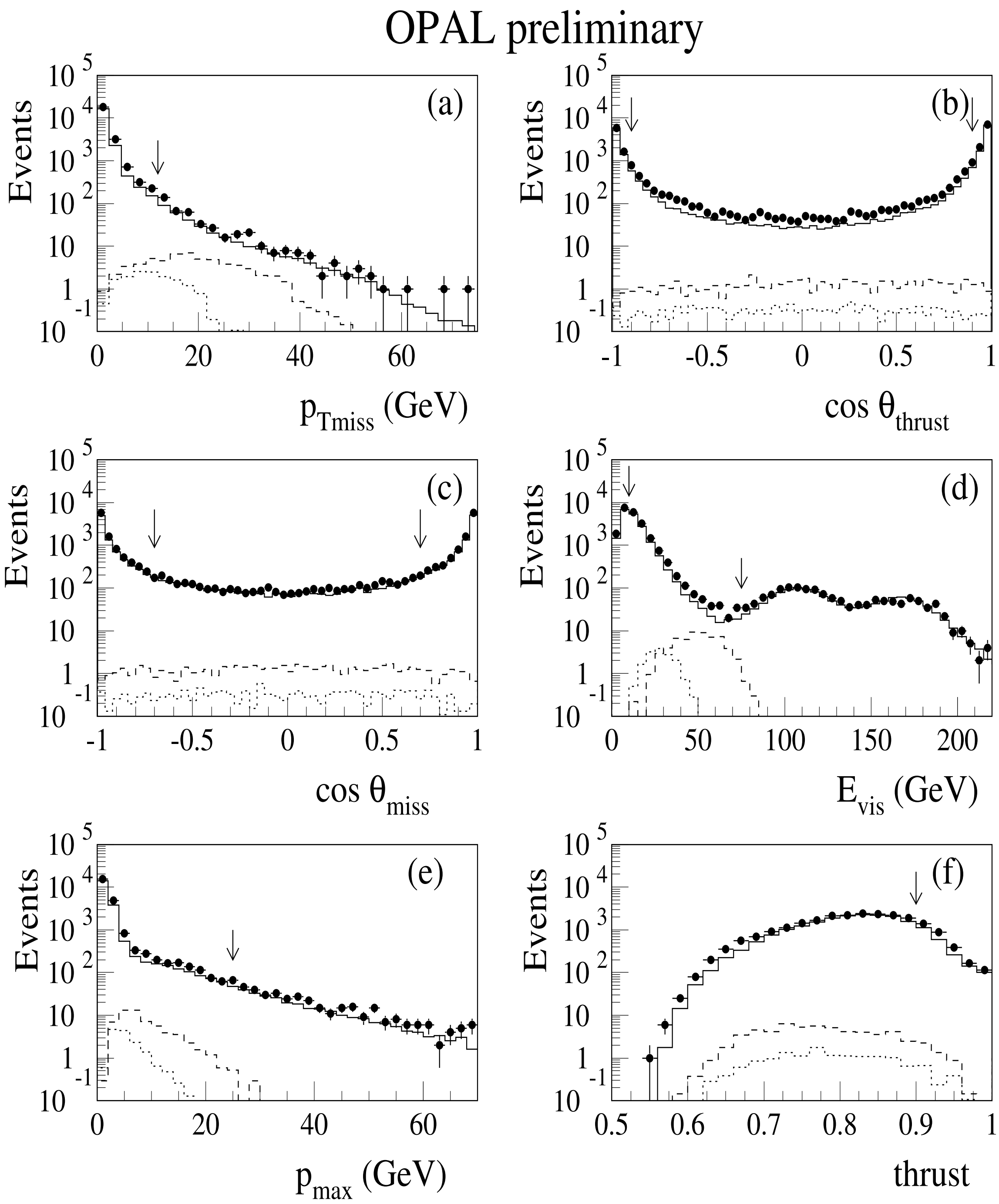

Figure 10: The plots show the distributions after cut (C1) for the data (points), the background processes (solid line), and the L^+L^- signal with $L^- \to N\,W^{-*}$ for the cases ($m_L = 75, m_N = 60$) GeV (dotted line) and ($m_L = 80, m_N = 50$) GeV (broken line $\times 5$) respectively for $\cos\theta_{\rm thrust}$ (a), $\cos\theta_{\rm miss}$ (b), $E_{\rm vis}$ (c), $p_{\rm Tmiss}$ (d), $p_{\rm max}$ (e), and the thrust value(f). The arrows correspond to the cut values.

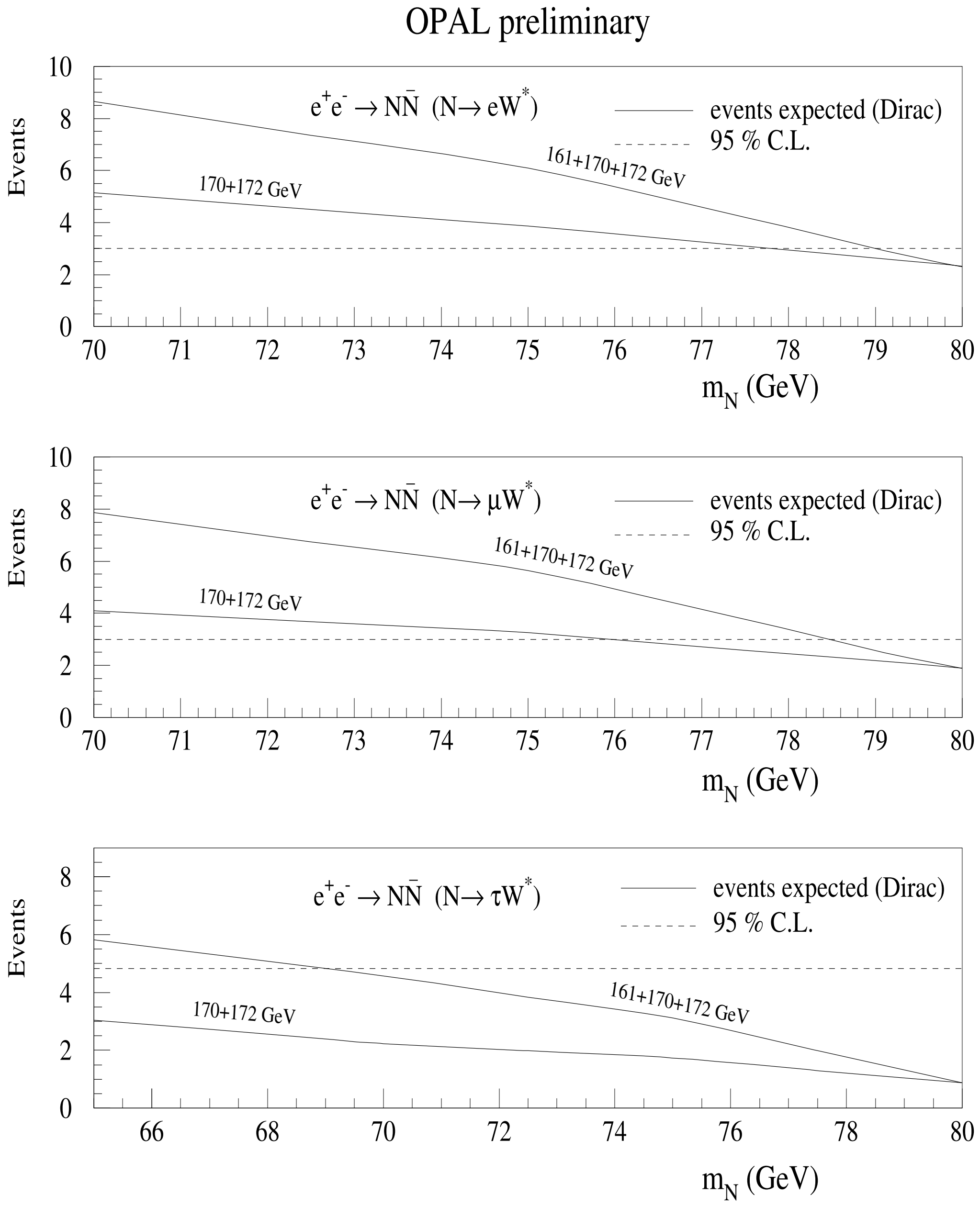

Figure 11: Expected number of events after all cuts for various masses and the 95 % C.L. limit for $\mathrm{N\bar{N}}$ (Dirac) production in the case where $\mathrm{N} \to \mathrm{e\,W}^*$, $\mathrm{N} \to \mu\,\mathrm{W}^*$, and $\mathrm{N} \to \tau\,\mathrm{W}^*$. The upper curve corresponds to the number of expected events when combining the results with those obtained at 161 GeV, while the lower curve is for 170 and 172 GeV data only.

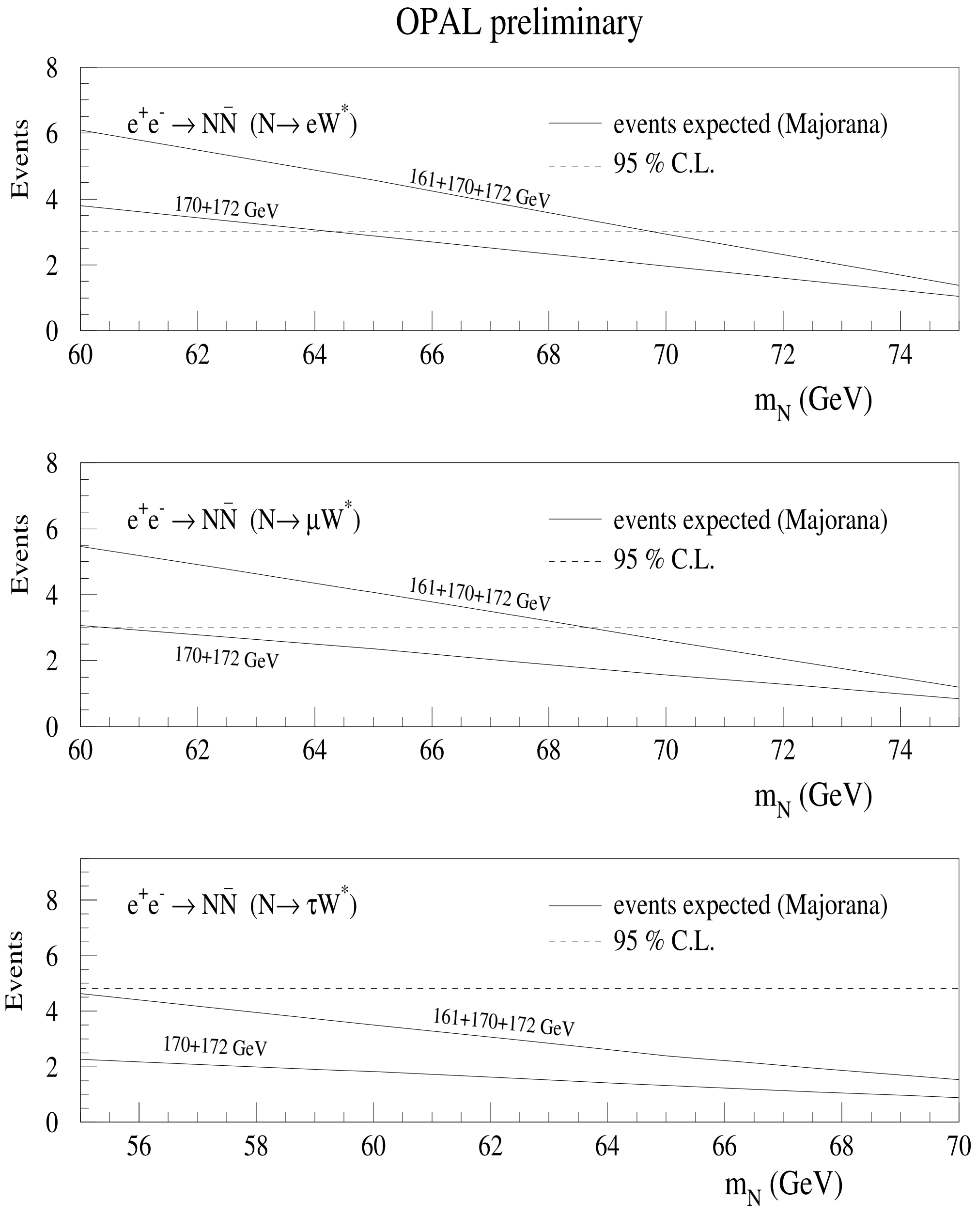

Figure 12: Expected number of events after all cuts for various masses and the 95 % C.L. limit for $N\bar{N}$ (Majorana) production in the case where $N \to e\,W^*$, $N \to \mu\,W^*$, and $N \to \tau\,W^*$. The upper curve corresponds to the number of expected events when combining the results with those obtained at 161 GeV, while the lower curve is for 170 and 172 GeV data only.

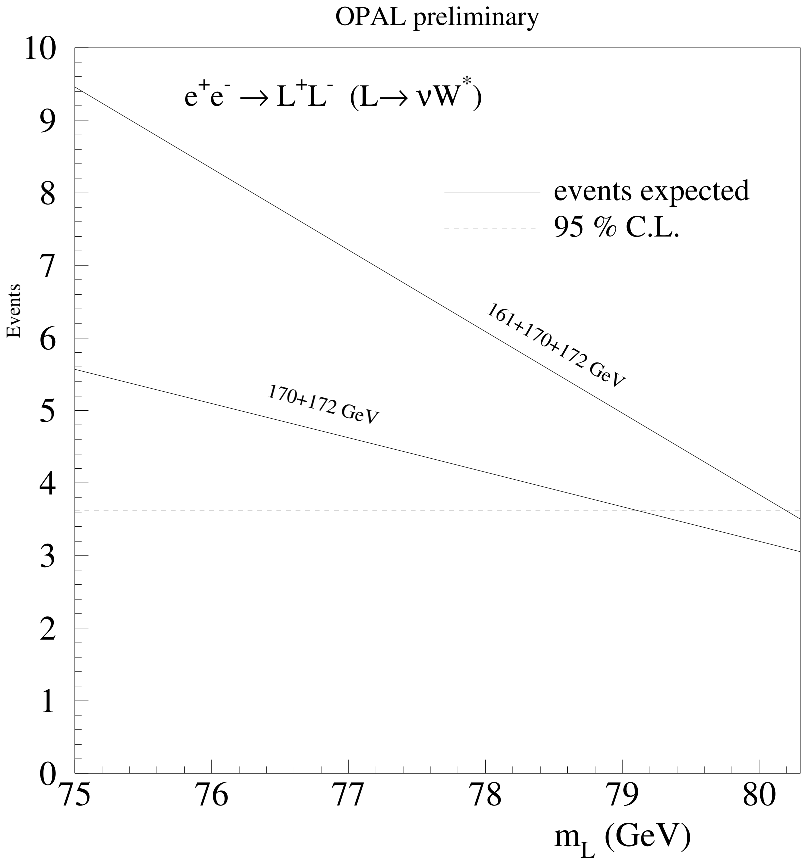

Figure 13: Expected number of events after all cuts for various masses and the 95 % C.L. limit for L^+L^- production in the case where $L^- \to \nu_\ell W^{-*}$. The upper curve corresponds to the number of expected events when combining the results with those obtained at 161 GeV, and the lower curve is for 170 and 172 GeV data only.

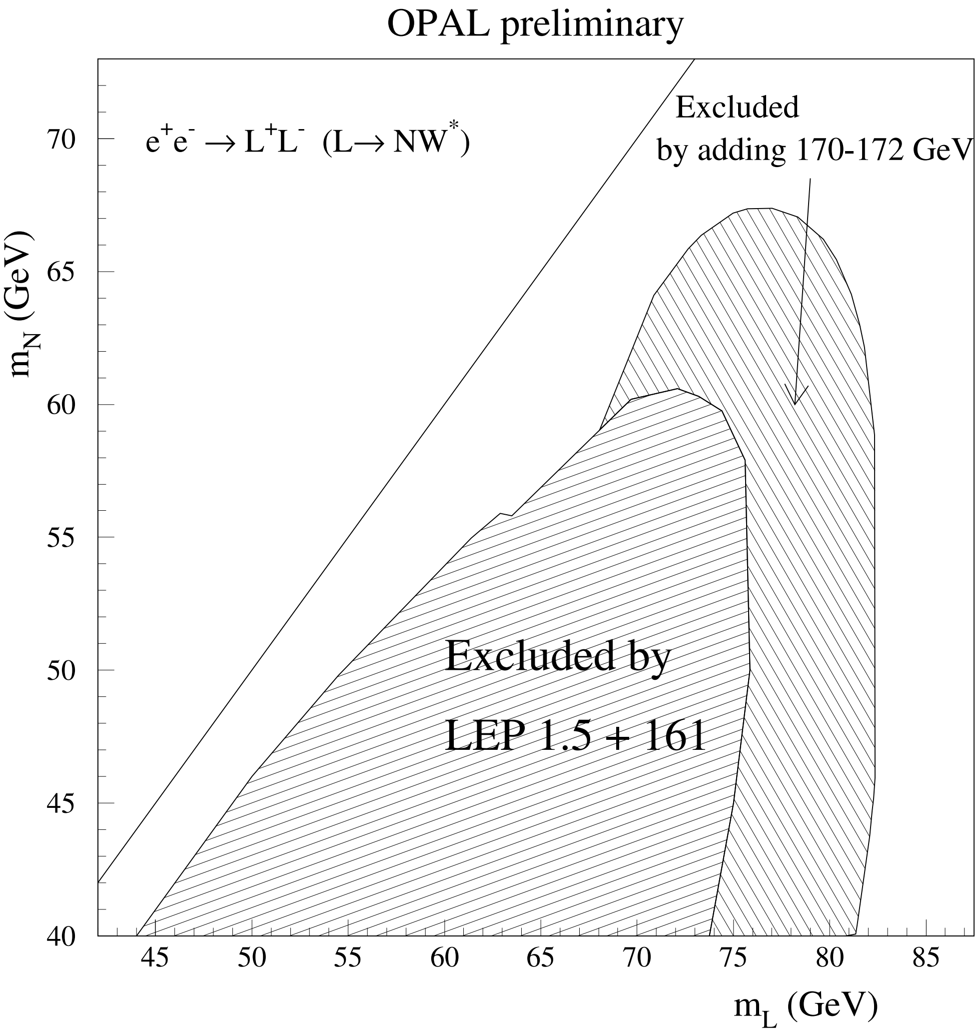

Figure 14: Excluded region in the $(m_{\mathrm{L}}, m_{\mathrm{N}})$ plane for $\mathrm{L}^+\mathrm{L}^-$ production in the case where $\mathrm{L}^- \to \mathrm{N\,W}^{-*}$ when combining the results with those obtained at 161 GeV. The diagonal line shows the kinematical limit.